Bio-Medical Materials and Engineering 24 (2014) 1751–1769
DOI 10.3233/BME-140987
IOS Press

Effect of sintering on the microstructural and mechanical properties of meleagris gallopova hydroxyapatite

S. Serdar Pazarlioglu [a,*], Hasan Gokce [b], Sevgi Ozyegin [c] and Serdar Salman [d]

[a] *Metal Education Department, Technical Education Faculty, Marmara University, Istanbul, Turkey*
[b] *Metallurgical and Materials Engineering Department, Istanbul Technical University, Istanbul, Turkey*
[c] *Department of Dental Technology, School of Health Related Professions, Marmara University, Istanbul, Turkey*
[d] *Mechanical Engineering Department, Faculty of Engineering and Architecture, Mehmet Akif Ersoy University, Burdur, Turkey*

Received 26 April 2013
Accepted 23 January 2014

Abstract. In this study, we obtained hydroxyapatite powders from the femur bones of meleagris gallopova at three steps and sintered at five different temperatures. The reactions, which occur during sintering of obtained powders, have been characterized by X-ray diffraction (XRD) patterns, scanning electron microscope (SEM), differential thermal analysis (DTA), thermogravimetric analysis (TGA) and Fourier transform infrared spectroscopy (FTIR) techniques. The mechanical properties of meleagris gallopova hydroxyapatite powders were determined by the measurements of density, hardness, porosity, activation energy for grain growth, variation of average grain sizes, fracture toughness and compression strength. The Fourier transform infrared spectra and the thermogravimetric analysis/differential thermal analysis thermograms of meleagris gallopova hydroxyapatite powders indicated that the presence of organic compounds were completely removed from the matrice. The X-ray diffraction patterns showed that decomposition of meleagris gallopova hydroxyapatite into tricalcium phosphate and calcium oxide was observed for the sintered samples at 1300°C. At the same temperature, formation of microcracks were also detected by scanning electron microscopy image. Mechanical tests showed that maximum hardness, fracture toughness and compression strength values were measured for the sintered samples at 1200°C.

Keywords: Meleagris gallopova, hydroxyapatite, sintering

1. Introduction

The number of treated skeletal deficiencies steadily increases in a global scale due to traffic accidents and/or injuries of sporting activities. Although autogenous bone is one of the most preferred for the treatment of bone defects, there are disadvantages and risks involved in using autogeneic bone such as post-operation pain, increased blood loss, secondary surgical wounds and risk of thrombosis. Allograft

*Address for correspondence: Metal Education Department, Technical Education Faculty, Marmara University, Goztepe Campus, 34722, Kadikoy, Istanbul, Turkey. Tel.: +90 216 336 57 70 (364); E-mail: spazarlioglu@marmara.edu.tr.

0959-2989/14/$27.50 © 2014 – IOS Press and the authors. All rights reserved

bone can overcome the above limitations, but it bears the risk of transmission of infection (e.g. HIV, Hepatitis, etc.). Another possible alternative for the treatment of bone defects is the use of effective and inexpensive biomaterials [1–3]. Hydroxyapatite [HA; chemical formula $Ca_{10}(PO_4)_6(OH)_2$] has been successfully applied in the medicine for several years due to its excellent biocompatibility, bioactivity, nontoxicity, noninflammatory and nonimmunogenicity properties. It has, therefore, been widely used in many medical applications. For example, porous hydroxyapatites have been used in bone ingrowth and sintered dense hydroxyapatites have been used for implants where the mechanical strength is one of the primary concerns. Furthermore, hydroxyapatite has also been used as a surface coating on many types of bioinert metallic and ceramic substrates, such as titanium and alumina [4,5]. Due to attractive properties of HA, various techniques have been developed. It can either be through chemical synthesis such as wet-precipitation [6,7], sol–gel method [8–10], solid-state reaction [11], hydrothermal method [12,13] and etc. It can also be synthesized from natural sources such as coral [14], egg shell [15], oyster shell [16], sheep [17], pig [18], fish [19] and bovine [20–23].

In the present study, hydroxyapatite powders were obtained from the femur bones of meleagris gallopova at three steps. Afterwards, meleagris gallopova hydroxyapatite powders (MGHAp) were compacted at 350 MPa and sintered at 900, 1000, 1100, 1200 and 1300°C for 4 h with the heating and cooling rates of 5°C/min in air atmosphere. Finally, the effect of sintering process on the microstructural and mechanical properties of MGHAp were investigated.

2. Experimental procedure

2.1. Obtaining of HA from femur bones of meleagris gallopova

In this study, meleagris gallopova femur bones (obtained from Banvit Company, Izmir, Turkey), were used as the raw material to produce HA powders. Femur bone samples were firstly cleaned to remove visible tissues and substances on the surface of bones and then head parts of the bones were cut off and marrow in shafts of all bones removed via boiling within water in a pressure cooker for 4 h to avoid soot formation during the calcination process [24]. After the boiling process, the retained shafts were deproteinized with sodium hidroxide (NaOH) for 1 h, washed with distilled water and then calcinated at 850°C with a heating rates of 5°C/min for 4 h to ensure that the organics are completely removed to eliminate any microbial contaminations [25]. The resulting white solid samples were firstly ground and then crushed in a mortar to produce hydroxyapatite powders between −63 μm to +45 μm. Then, they were ball milled in a zirconia coated container by zirconia balls and ethanol in Restch PM 100 ball milling device at 150 rpm for 8 h until fine powder was obtained as shown in Fig. 1. After the ball milling process, the powders were dried at 105°C for 24 h and exposed to X-ray diffraction to confirm the presence of HA into obtained powders.

2.2. Sintering of the MGHAp

Green body pellets about 2 grams with the dimensions of 12 mm height and 8 mm diameter were compacted by uniaxial cold pressing in hardened steel dies according to procedure described in the literature [26]. Finally, the compacted green samples were sintered at 900, 1000, 1100, 1200 and 1300°C for 4 h with the heating and the cooling rates of 5°C/min in Nabertherm LHT 12/70 furnace.

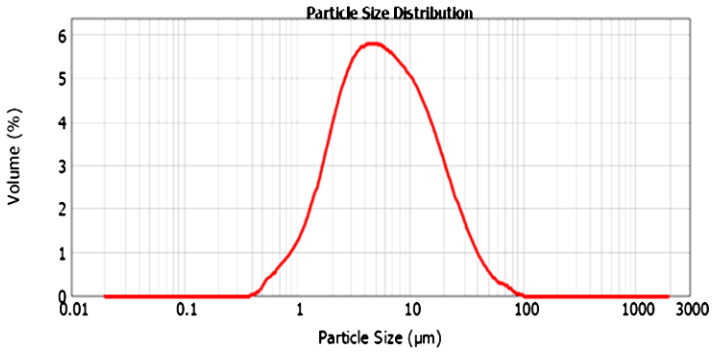


Fig. 1. Particle size distribution of MGHAp after ball milling process. (Colors are visible in the online version of the article; http://dx.doi.org/10.3233/BME-140987.)

2.3. Microstructural characterization

The X-ray diffraction (XRD) patterns were obtained at room temperature in an X'Pert MPD Philips diffractometer using Cu–Kα radiation at 40 kV and 30 mA. Intensity data were collected by step counting method (step 0.02° and a time per step of 0.6 s) in the range of 2° (10–80°). The microstructures of the samples were determined by scanning electron microscope (SEM, JOEL Ltd., JSM-5910 LV), equipped with energy dispersive spectroscopy (EDS, Oxford Industries INCAx-Sight 7274, 133-Ev resolution 5.9 keV) for elemental analysis after gold coating. Fourier transform infrared (FTIR) spectroscopy was employed in the range of 4000–400 cm^{-1} to characterize the functional groups of MGHAp. Differential thermal analysis (DTA) was carried out at the heating rate of 5°C/min between room temperature and 1300°C (Perkin Elmer PE-7 Series, USA) for the powders obtained from the femur bones of meleagris gallopova before the obtaining of hydroxyapatite powders to determine optimum calcination temperature and also to be sure whether the organics are completely removed to eliminate any microbial contaminations or not. α-alumina was used as reference material. Thermogravimetric analyzer (TGA) was used to find the weight loss during heating at the same device. Average grain sizes of sintered samples were measured by lineal intercept method using SEM images. The activation energy for grain growth was determined from the grain size measurements by constructing an Arrhenius plot for a constant sintering time. The best fit line was plotted by using the least minsquare method. The slope of this line was used to determine the activation energy (Q) from the Eq. (1):

$$D = A \exp[Q/RT], \tag{1}$$

where D is the average grain size, T is the temperature and R is the gas constant, i.e. 8.314 kJ/kmol K [27].

2.4. Mechanical tests of MGHA

For the density and porosity measurements, the sintered samples were initially subjected to ultrasonic washing in distilled water for a few minutes. After drying, the samples in a stagnant air oven at 90°C, their dry weights were recorded. The samples were then boiled in distilled water for about 3 h, and allowed to cool in water for 24 h. Wet weight in air and wet weight suspended in water were determined by

using an analytical balance (Precisa, 300S, Switzerland). Bulk density and apparent porosity of sintered samples were calculated using the Eqs (2) and (3), respectively.

$$\text{Bulk density:} \quad D/(W-S), \tag{2}$$

$$\text{Apparent porosity:} \quad (W-D)/(W-S), \tag{3}$$

where D is the dry weight of the samples, W is the wet weight of the samples and S is the wet weight suspended in the water of the samples [28]. The relative densities of sintered samples were calculated by taking the theoretical density of HA as 3.156 g cm^{-3}. The compression strengths of the sintered samples were measured using Devotrans Universal testing device at 2 mm/min speeds. Micro-vickers indentation method was used to determine the hardness and fracture toughness (K_{IC}) of the sintered samples. Loads of 1.962 N for 20 s and 2.943 N for 30 s were applied to measure hardness and fracture toughness, respectively. Prior to indentation, the surface of the samples were polished to 3 μm diamond paste. Twenty measurements were performed on each samples both microhardness and fracture toughness measurements. For the calculation of microhardness values of each samples Eq. (4) was used:

$$HV: \quad 0.001854\frac{P}{d^2}. \tag{4}$$

Fracture toughness of the samples was determined according to the length of the cracks generated by the indentations applied during the micro-hardness test. Two widely used equations were used to calculate the fracture toughness. Depending on the size of the cracks formed by indentation, one equation (Eqs (5) or (6)) was preferred.

$$K_{IC}: \quad 0.0824\frac{P}{c^{3/2}}, \tag{5}$$

where K_{IC}: Fracture toughness (MPa $\cdot$ $m^{1/2}$), P: Applied load (N), c: Crack length (m).

$$K_{IC}: \quad 0.035\left(\frac{E^{0.4}H^{0.6}}{\phi^{0.6}}\right)\left(\frac{a}{(c-a)^{0.5}}\right), \tag{6}$$

where H: Hardness (MPa), E: Elastic modulus (MPa), ϕ: the coefficient related to material constraint ($\equiv$3) [29].

3. Results and discussions

The TG and DTA thermograms of the powders obtained from the femur bones of meleagris gallopova before calcination process are shown in Fig. 2. As indicated in literature, two types of water exists in apatite structure: absorbed and lattice water [30]. In the present study, the weight loss of the MGHAp occurred in three steps. The first loss is due to the removal of absorbed water in the MGHAp between room temperature to 346.20°C. In the second step, the decomposition of lattice water molecules occurred between 346.20°C to 460.60°C. In the third step, losses resulted from the burning of organic components occurred between 460.60°C to 850°C in the MGHAp. No significant weight loss was observed between 600°C and 850°C, indicating the complete removal of organic materials.

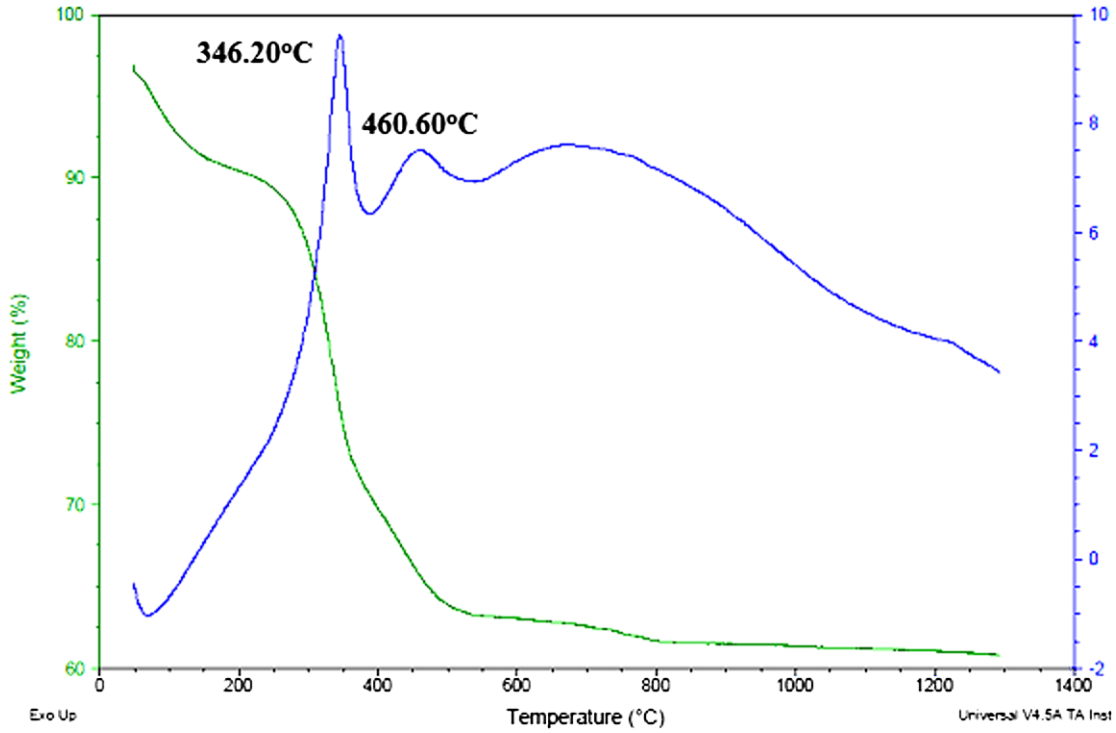
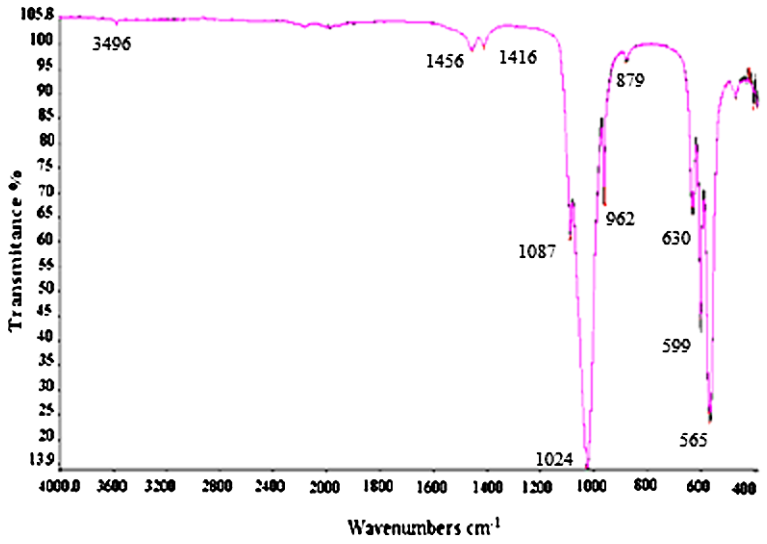


Fig. 2. The TG and DTA thermograms of the powders obtained from the femur bones of meleagris gallopova before calcination process. (Colors are visible in the online version of the article; http://dx.doi.org/10.3233/BME-140987.)

The FTIR spectrum of MGHAp before sintering showed absorptions at 3496, 1456, 1416, 1087, 1024, 962, 879, 630, 599 and 565 cm^{-1} that were attributed to carbonate (CO_3^{-2}), phosphate (PO_4^{-3}), hydroxyl (O–H) and carbon dioxide (CO_2) as shown in Fig. 3(a). The absorption peaks of 3496 and 630 cm^{-1} were caused by stretching vibration of the O–H group. As a major peak of phosphate group, the $\nu 3$ vibration peaks could be identified at 1087 and 1024 cm^{-1}, the $\nu 1$ absorption band at 962 cm^{-1} and the $\nu 4$ absorption bands at 599 and 565 cm^{-1} were due to symmetric P–O stretching vibration of PO_4^{-3} group [31]. The stretching modes of the carbonyl from the CO_3^{-2} groups which are seen at between 1456 and 1416 cm^{-1} to be $\nu 4CO_3^{-2}$ and 879 cm^{-1} to be $\nu 2CO_3^{-2}$ [32]. The presence of peak in the region 2000–2400 cm^{-1} was due to absorbed CO_2 [33]. The FTIR spectrum of the samples sintered at 900°C exhibit absorption bands at 1087, 1025, 960, 596 and 565 cm^{-1} which are assigned to the PO_4^{-3} ions. In addition, the spectrum show absorption peaks at 1456, 1408 and 960 cm^{-1} which correspond to the vibrations of the CO_3^{-2} and also peaks at 3496 and 627 cm^{-1} which correspond to the vibrations of the OH^-. Based on the FTIR spectra, it can be concluded that no significant changes in the shapes and intensities of the individual bands characteristic for HA can be observed for the sintered sample at 1000 and 1100°C. Within the temperature range between 900°C and 1000°C, amount of CO_3^{-2} groups in the samples reduces and bands of CO_3^{-2} group fully disappear at 1100°C.

When the sintering temperature reaches 1200°C, the band at 627 cm^{-1} originating from the libration bands of OH^- groups of MGHAp disappears, whereas the band at 3496 corresponding to the stretching vibrations of the OH^- becomes flat and the formation of β-TCP detected at 436 cm^{-1}. The FTIR spectrum of samples sintered at 1300°C exhibit absorption bands at 1019, 596 and 565 cm^{-1} which



(a)

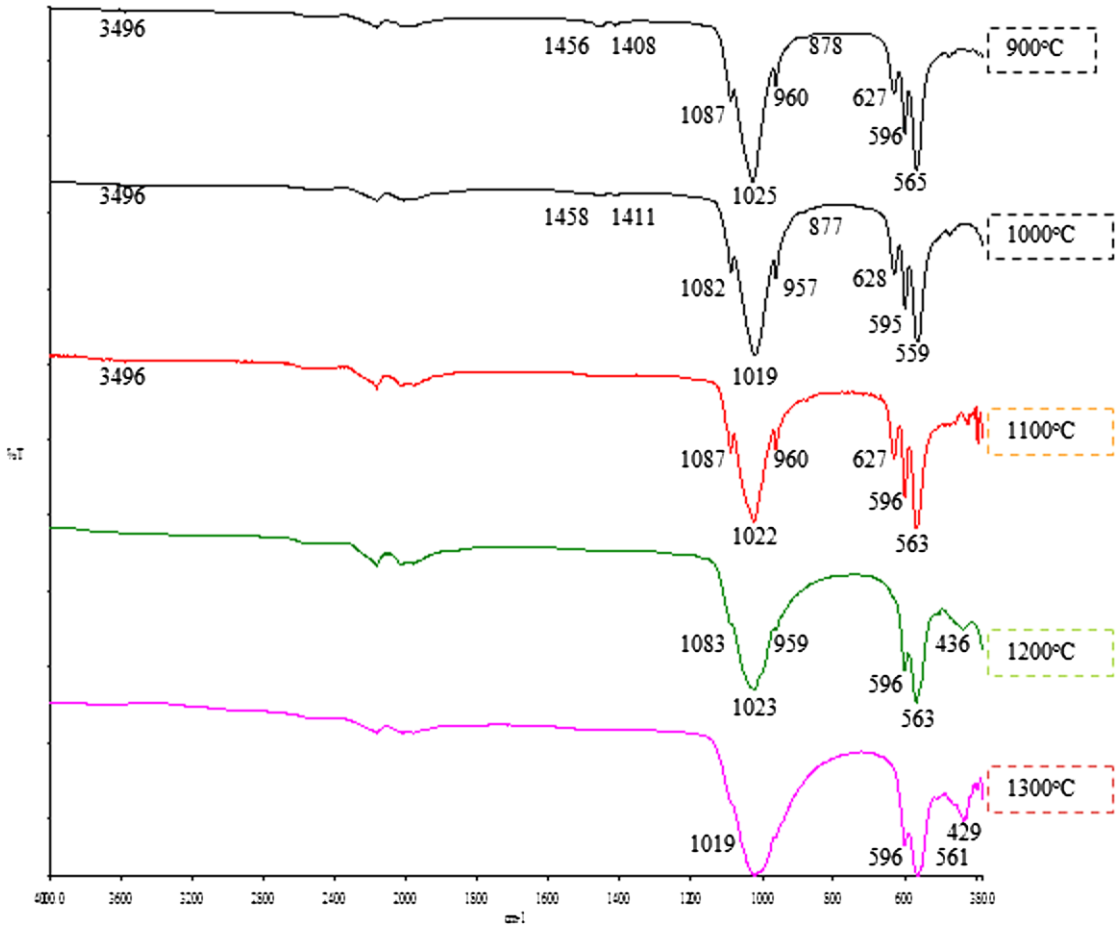
Fig. 3. (a) FTIR spectrum of MGHAp at room temperature. (Colors are visible in the online version of the article; http://dx.doi.org/10.3233/BME-140987.)

are assigned to the PO_4^{-3} ions. In addition, the spectrum show absorption peaks at 429 cm^{-1} which correspond to the vibrations of the β-TCP [34].

Figure 4(a)–(e) illustrate the XRD patterns of obtained MGHA powders from the femur bones of meleagris gallopova and sintered MGHA powders at different sintering temperatures, respectively. As can be seen in Fig. 4(a)–(d) the most important peaks of HAP were observed in all samples with no additional peaks correspond to other calcium phosphates. The obtained peaks at 2θ of 25.9 (002), 31.8 (211), 32.23 (112), 32.96 (300), 34.1 (202), 39.83 (130), 46.74 (222) and 49.51 (213) were in concurrence with the ICDD card No. 09-432 for HAp. In the present study, the MGHA crystallized in the hexagonal space group of $P_{6/3m}$ with $a = b = 9.415$ and $c = 6.879$, $\alpha = \beta = 90°$, $\gamma = 120°$ and $Z = 1$. Sintering of HA is complicated by two processes, namely dehydroxylation and decomposition at elevated temperatures. During dehydroxylation, HA loses OH radicals upon heating according to the Eq. (7):

$$Ca_{10}(PO_4)_6(OH)_2 \longrightarrow Ca_{10}(PO_4)_6(OH)_{2-2x}O_x\square_x + xH_2O, \tag{7}$$

where $\square$ stands for a vacancy. In the limit, when $x = 1$, oxyapatite ($Ca_{10}(PO_4)_6O$, OAP) is formed [35]. The HAp dehydroxylation does not occur instantly but over a wide temperature range, which has been reported to mainly depend on the partial H_2O pressure during heating. If performed under vacuum, HAP loses its OH^- at a lower temperature, about 850°C. If HAP is heated in a H_2O stream, the structure of HAP is then preserved up to 1100°C [36]. This condition was also observed for our study which may related to the high humid atmosphere (the relative humidity is higher than 75% all year around [37]) could have facilitated sintering by providing sufficient water vapour in the furnace atmosphere. In this study, it is difficult to observe HAP transformation to OHAP by XRD because most of the characteristic peaks of the two compounds overlap one another. The presence of OHAP in MGHAp can, however, be detected by FTIR as show in Fig. 3(b) for sintered samples at 900°C, 1000°C and 1100°C. MGHAp has two types of OH^- band and librational absorption bands at 3496 and 630 cm^{-1}, respectively. As shown



(b)

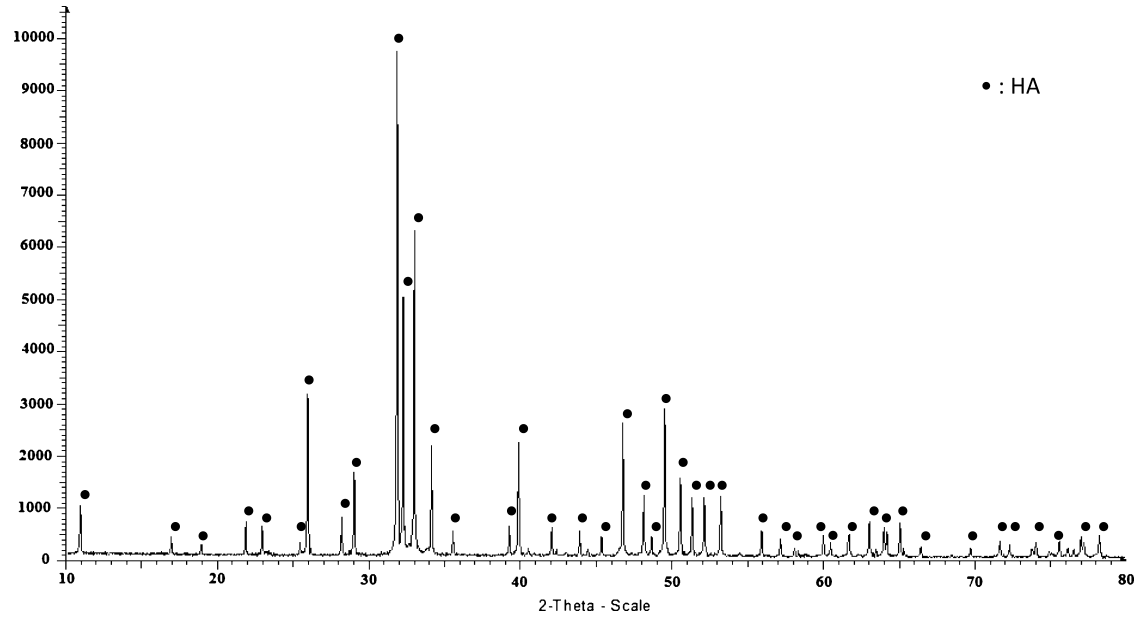
Fig. 3. (*Continued.*) (b) FTIR spectrums of sintered MGHAp at 900°C, 1000°C, 1100°C, 1200°C and 1300°C. (Colors are visible in the online version of the article; http://dx.doi.org/10.3233/BME-140987.)

in Fig. 3(b), the intensity of the peak at 630 cm^{-1}, which corresponds to the OH^- librational mode diminishes with a temperature increase until 1200°C where it disappears. Figure 4(e) shows the presence of two phases: β-TCP (JCPDS 9-169) and HA. Four main peaks were observed for β-TCP at 2θ angle of 34.086, 31.529, 40.826 and 46.735 while for HA, they were observed at 2θ of 25.87, 32.20, 31.82 and 32.97. The highest peak intensities for β-TCP and HA were at 34.086 and 31.823 corresponding to the plane (110) and (211) for the sintered sample at 1200°C, respectively. The presence of CaO which was detected by XRD (JCPDS no. 75-0264), as shown in Fig. 4(e), when sintered at 1300°C could be attributed to an alternative decomposition route according to the following reaction [38]:

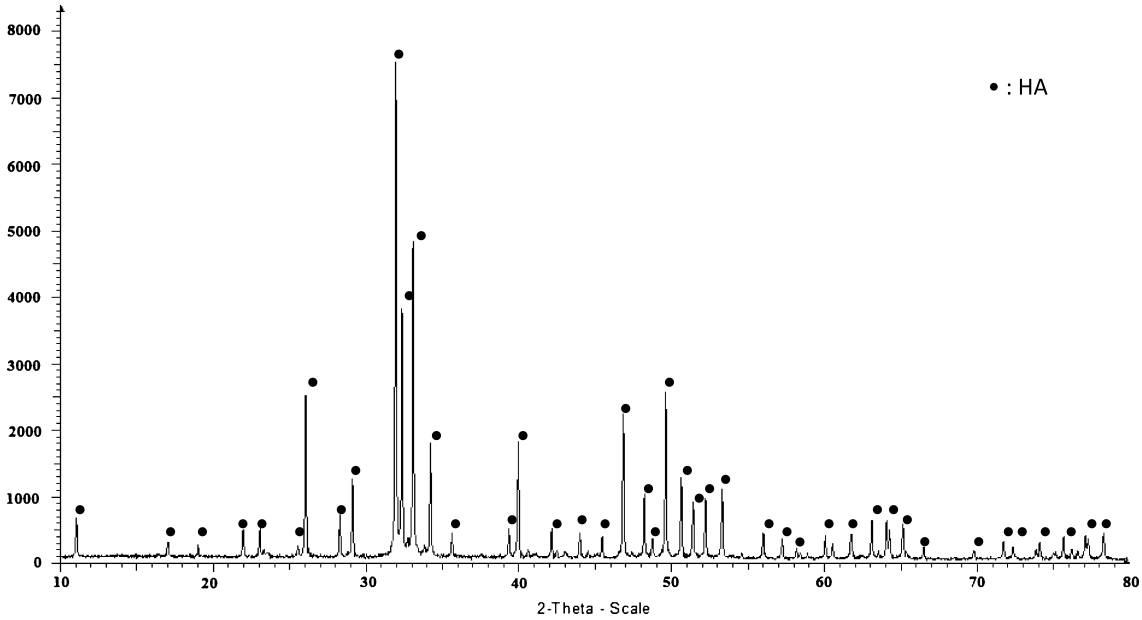
$$Ca_{10}(PO_4)_6(OH)_2 \longrightarrow 3Ca_3(PO_4)_2 + CaO + H_2O. \tag{8}$$

These data indicate that hydroxyapatite got decomposed into β-TCP and CaO.

In general, during solid state sintering of powder compacts, the pore size and morphology evolves through three stages: (i) an initial stage when necks start to form and grow between particles, (ii) an



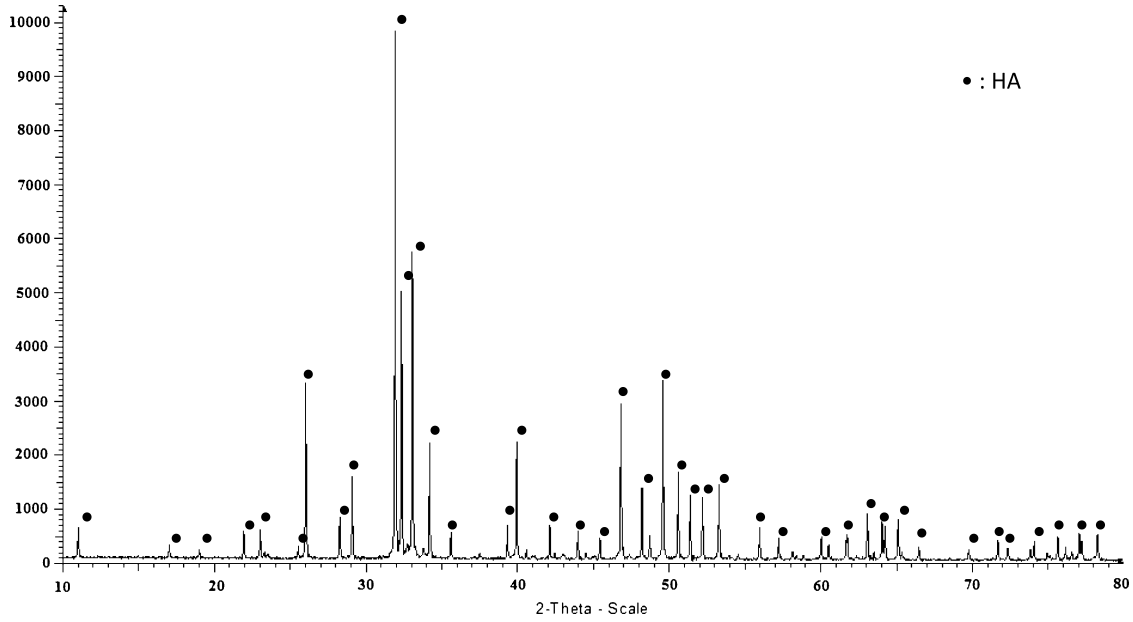
(a)



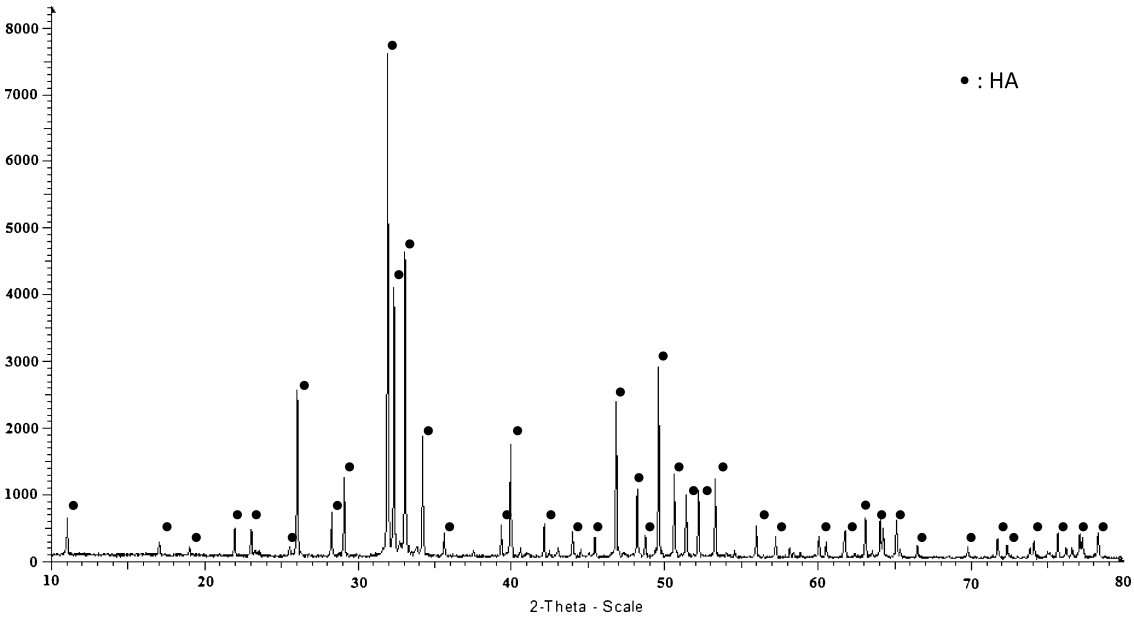
(b)

Fig. 4. XRD patterns of obtained MGHA powders from the femur bones of meleagris gallopova (a) and sintered MGHA powders at (b) 900°C, (c) 1000°C, (d) 1100°C, (e) 1200°C and (f) 1300°C.

intermediate stage where tubular pores appear along the grain boundaries and (iii) a final stage at which the tubular pores break up into isolated quasi-spherical pores typically located at the triple points of grains [39]. These typical microstructural evolutions were observed for MGHAp in this study as shown in Fig. 5(a)–(e). When the pellets of MGHAp sintered at 900°C, local interconnections between grains



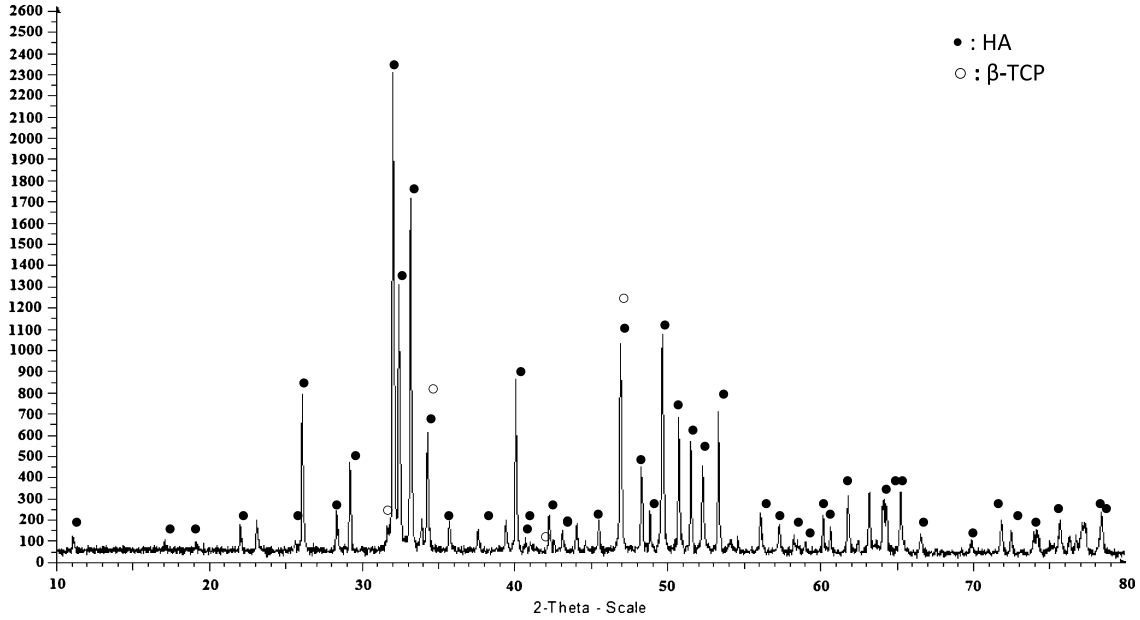
(c)



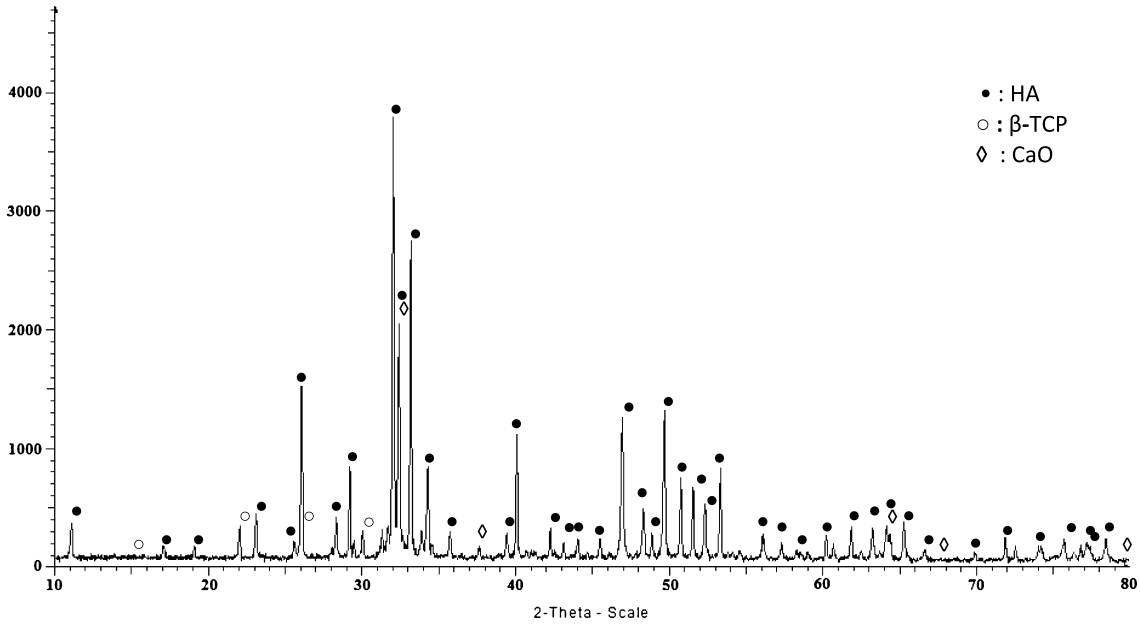
(d)

Fig. 4. (*Continued*.)

via necks and also large cavities due to open networks of pores were observed as shown in Fig. 5(a) and (b). Figure 5(b) shows a denser structure sintered after 1000°C and the average grain size 4.32 μm was slightly larger than that of the compact sintered at 900°C (2.75 μm). During the intermediate sintering stage, not only the most densifications occurred, but also pore size, number density of pores and pore morphology underwent significant changes. This event was determined for MGHAp sintered at



(e)



(f)

Fig. 4. (*Continued*.)

1100°C (5.80 μm) as shown in Fig. 5(c). In the final stage, no porosity is found on the surface of sintered samples at 1200 and 1300°C. The grain size of the sintered at 1200°C sample is about 8.8 μm as shown in Fig. 5(d). Considerable grain growth (13.6 μm) and microcracks, which may related to much larger difference in coefficient of thermal expansion (CTE) between second (TCP) or third (CaO) phases and HA, observed for the samples sintered at 1300°C as shown in Fig. 5(e).

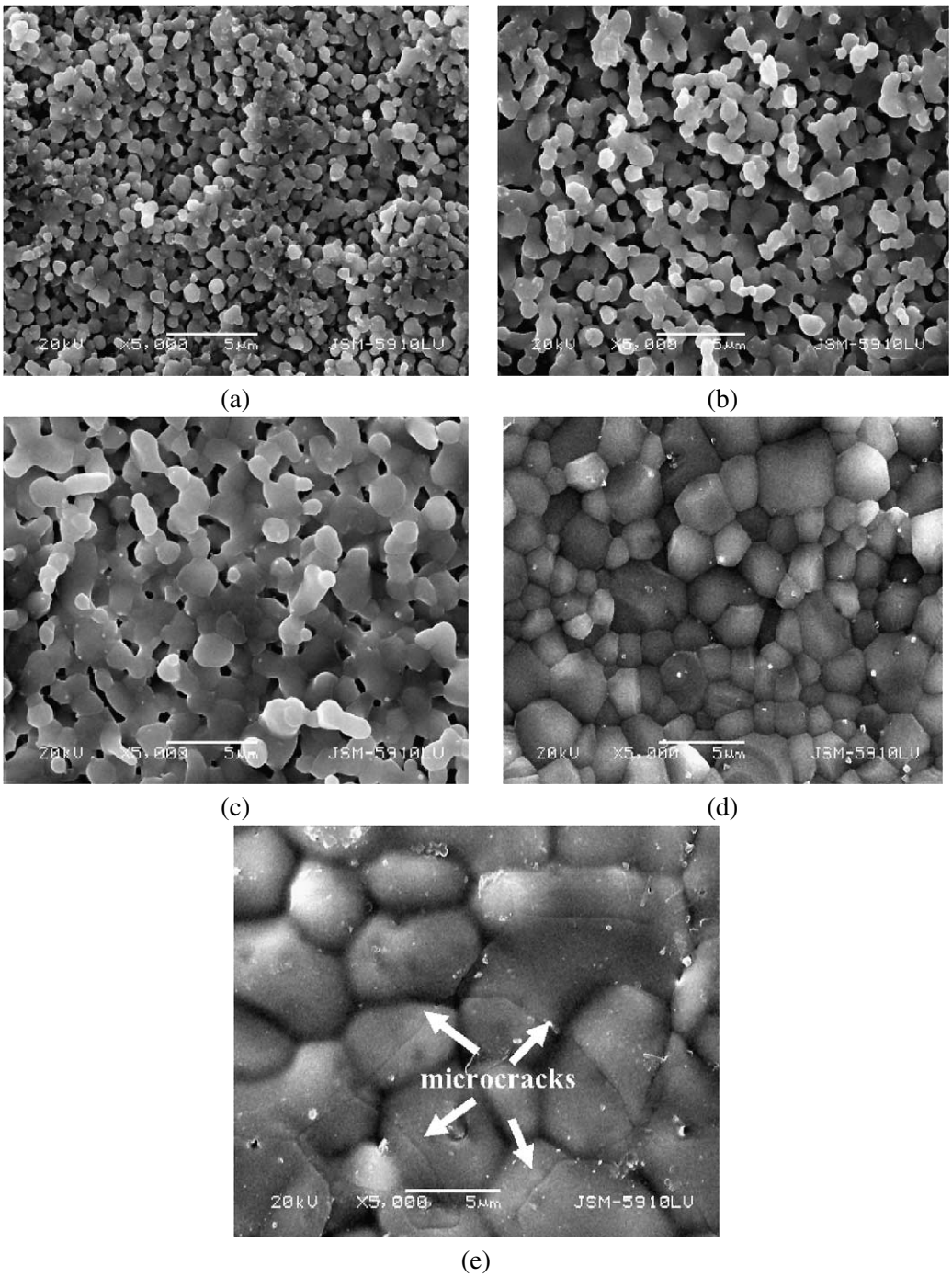


Fig. 5. SEM images of MGHA sintered at (a) 900°C, (b) 1000°C, (c) 1100°C, (d) 1200°C and (e) 1300°C.

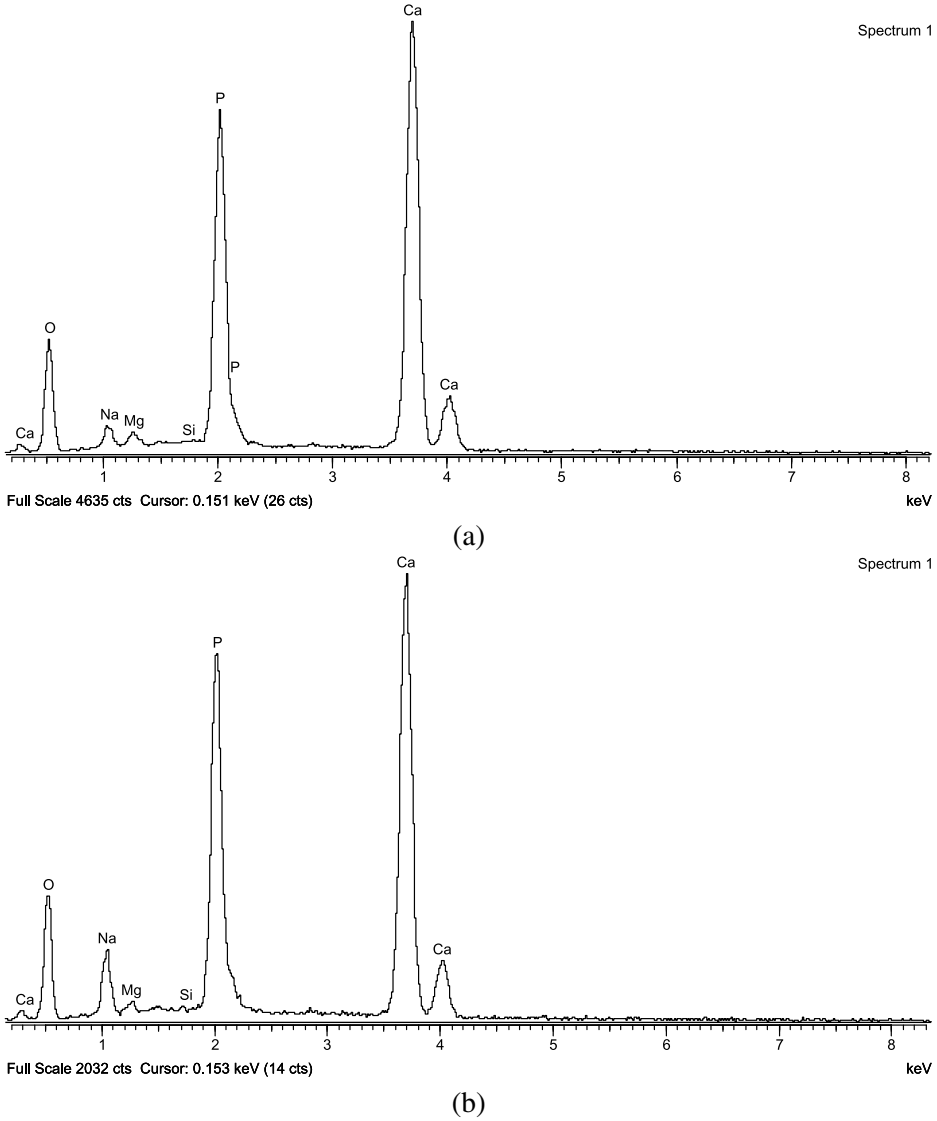
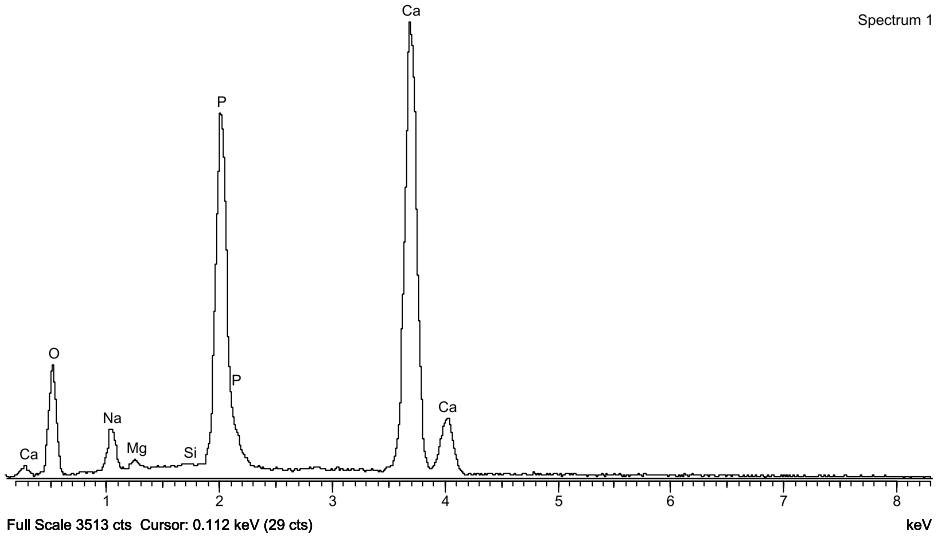


Fig. 6. EDS analysis of MGHA sintered at (a) 900°C, (b) 1000°C, (c) 1100°C, (d) 1200°C and (e) 1300°C.

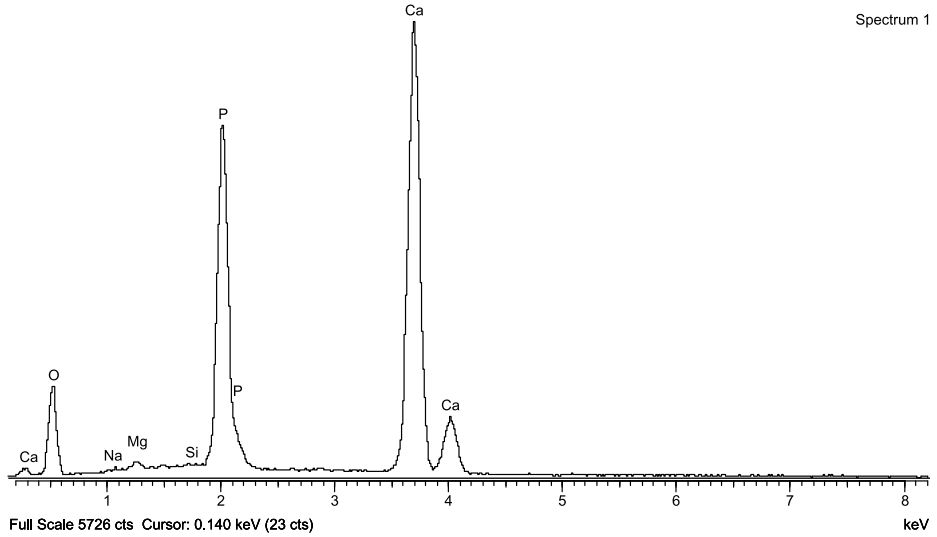
EDS analyses showed that inorganic phases of sintered MGHAp were mainly composed of calcium and phosphorus as major constituent with some minor components such as oxygen, sodium, magnesium and silica (Fig. 6(a)–(e)).

The activation energy for grain growth was determined from the grain size measurements by constructing an Arrhenius plot for a constant sintering time as shown in Fig. 7. The value for Q obtained from this plot for grain growth in hydroxyapatite was 61 kcal/mol. This value for diffusion in HA is in agreement with values reported by Muratlithran and Ramesh [27] and their referred values such as 47 kcal/mol, 56 kcal/mol and 57 kcal/mol.

Figure 8 shows the effect of sintering temperatures on the porosity rates (%) and density (g/cm^3) of the sintered MGHAp. It was found that porosity rates (%) of MGHAp decreased from 30.340 ± 2.502



(c)

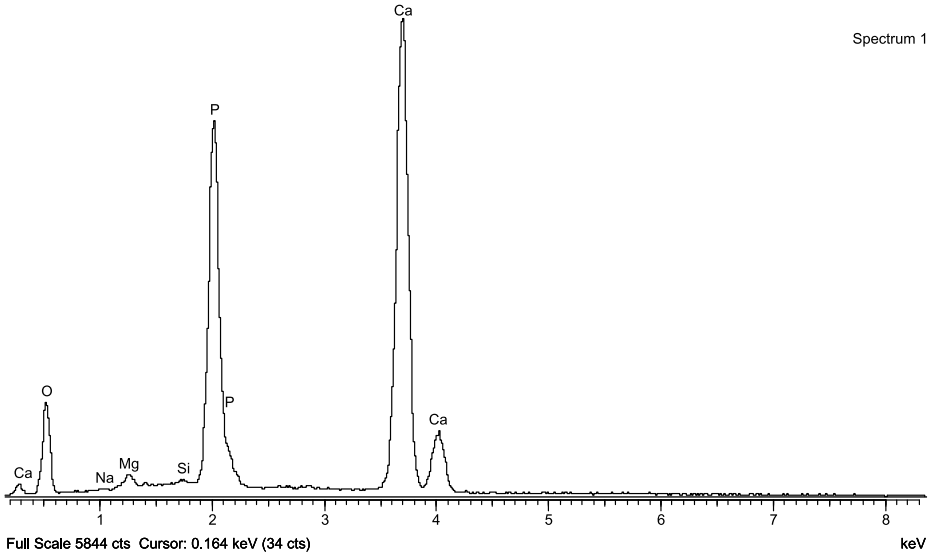


(d)

Fig. 6. (*Continued*.)

to 2.239 ± 0.745 by increasing sintering temperatures. Moreover, increasing the sintering temperature leads to decrease of porosity and increase of density. Raising the sintering temperature results in the increment of density at first, but there is an end density at 1200°C (2.897 ± 0.035). The density does not increase significantly over this end value despite sintering at higher temperature (2.944 ± 0.045). So densification appears to be completed near 1200°C with a measured relative density higher than 91%. These measured densities are high and are not in agreement with some of values reported in the literature for biologically derived hydroxyapatite ceramics sintered up to 1300°C [1,40].

The relative densities and micro-vickers hardness of the sintered samples are shown as a function of sintering temperature in Fig. 9. It can be noted that the lowest hardness values of 0.654 ± 0.035 GPa



(e)

Fig. 6. (*Continued*.)

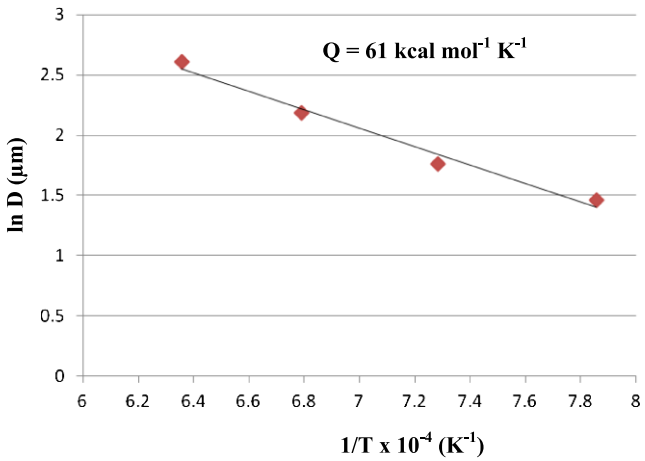


Fig. 7. Arrhenius plot of log mean grain size against reciprocal of sintering temperature for MGHA. (Colors are visible in the online version of the article; http://dx.doi.org/10.3233/BME-140987.)

was measured for the sintered sample at 900°C (with relative density of 68.85 ± 1.004), whereas the maximum hardness value of 2.16 ± 0.600 GPa was obtained for the sintered sample at 1300°C (with relative density of 93.30 ± 1.454). According to Fig. 8, the hardness increases slowly from 900 to 1000°C and then increase rapidly by a factor of more than 330%, when the temperature was increased from 900 to 1300°C. The slowly increasing in the hardness at 1300°C compared to 1200°C may be due to existence of closed porosity, increased grain size and/or formation of glassy phases around grains [41].

The fracture toughness and the micro-vickers hardness of sintered samples are shown as sintering temperatures in Fig. 10. Both fracture toughness and hardness increase with increasing temperatures up to 1200°C. The samples sintered at 1200°C shows a maximum fracture toughness of 0.935 ±

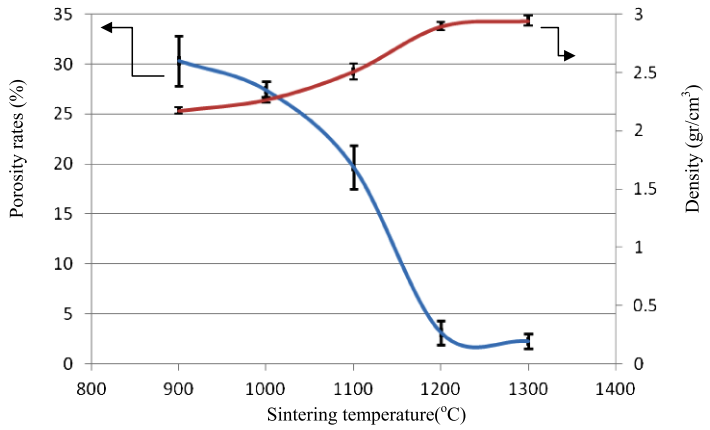


Fig. 8. The effect of sintering temperatures on the porosity (%) and density of the sintered MGHAp. (Colors are visible in the online version of the article; http://dx.doi.org/10.3233/BME-140987.)

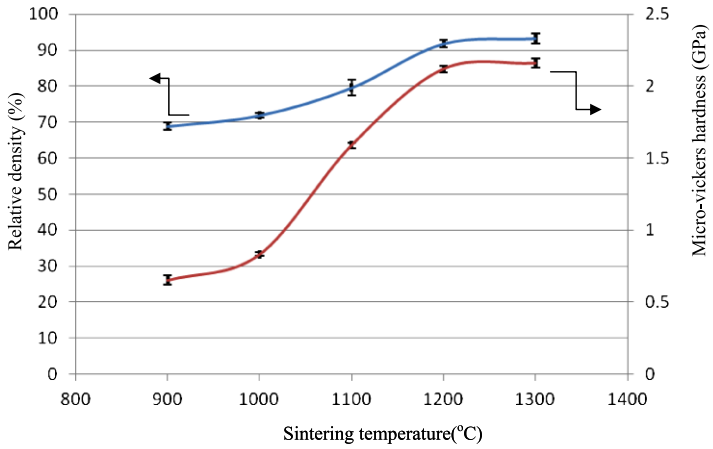


Fig. 9. The relative densities and micro-vickers hardness of the sintered samples as a function of sintering temperature. (Colors are visible in the online version of the article; http://dx.doi.org/10.3233/BME-140987.)

0.101 MPa · $m^{1/2}$ and then decrease to 0.909 ± 0.80 MPa · $m^{1/2}$ for the sintered samples at 1300°C. This is due to the fact that the density increase slightly and the extremely grain size grows from 8.8 to 13.6 μm. A decrease of fracture toughness with extremely increasing grain size is usually observed in compacts when the mechanism is transgranular because to major contribution to cracking resistance is related to the crossing of grain boundaries [42].

The compression strength and fracture toughness of sintered samples are shown in Fig. 11. It is well known that the compression strength of HA ceramics depend on many parameters such as preparation conditions, methods of pre-sintering compaction, sintering time and temperature, porosity, microstructure (grain size and pore shapes) degree of high temperature decomposition of the HA, etc. Moreover, the compressive strength can widely vary even for specimens prepared by the same method [43]. The compression strength of the sintered samples at 900°C was too low due to the insufficiently high sintering temperature. However, as the sintering temperature increased to 1200°C, the maximum value occurs. Also, the fracture toughness exhibit same regime. This result suggests that powders used in this study

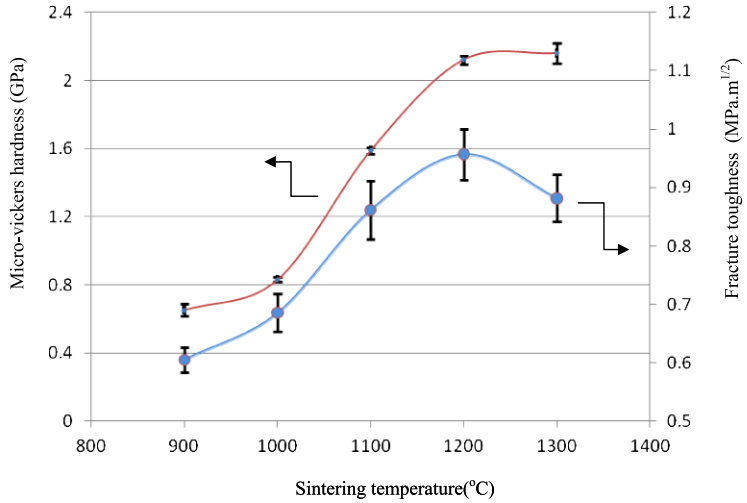


Fig. 10. The micro-vickers hardness and fracture toughness of the sintered samples as a function of sintering temperature. (Colors are visible in the online version of the article; http://dx.doi.org/10.3233/BME-140987.)

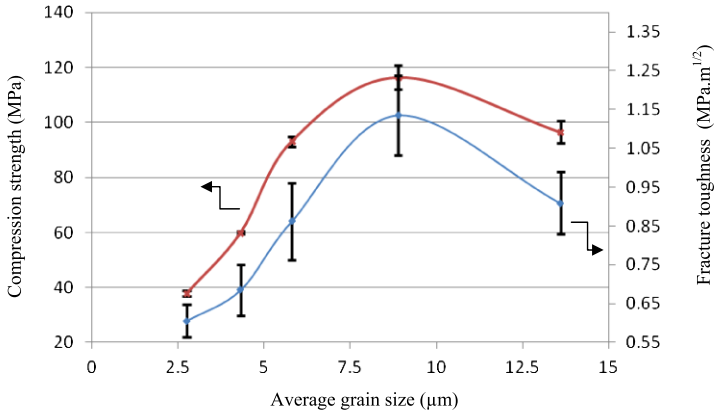


Fig. 11. The compression strength and fracture toughness of the sintered samples as a function of average grain size. (Colors are visible in the online version of the article; http://dx.doi.org/10.3233/BME-140987.)

show better consolidation properties at higher temperatures. The reduction of compression strength of MGHAp samples sintered at 1300°C may due to the decomposition of HA into β-TCP and CaO which was described in Fig. 4(e) and extremely grain growth.

Compared to early studies carried out with the HA powders derived from biological sources and then pelleted according to British 7253 standard (Table 1) density, microhardness and compressive strength of MGHAp are generally higher than the others. This higher mechanical properties for MGHA may be related to the dissimilar calcination temperature and time used during MGHAp production and also average grain size of starting powders. However, it is also seen from Table 1 that MGHA and BHA powders [44] are stable until 1200°C, SHA and CHA [17] are stable at higher temperature. This condition explained on page 1755, on page 1757 and on pages 1758–1760 respectively using FTIR, XRD and SEM analysis.

Table 1
Comparison of the mechanical properties of MGHAp with other biologically derived HA powders

T (°C)	Meleagris Gallopova Hydroxyapatite (MGHA) (Present study)			Bovine Hydroxyapatite (BHA) [43]			Chicken Hydroxyapatite (CHA) [44]			Sheep Hydroxyapatite (SHA) [17]		
	ρ (g/cm^3)	δ_C (MPa)	HV	ρ (g/cm^3)	δ_C (MPa)	HV	ρ (g/cm^3)	δ_C (MPa)	HV	ρ (g/cm^3)	δ_C (MPa)	HV
900	2.173	37.8	66.0	–	–	–	–	–	–	–	–	–
1000	2.268	59.9	83.3	1.98	12	42	2.22	40.2	101.4	2.09	31	49
1100	2.510	93.1	160.7	2.59	23	92	2.38	63.2	171	2.16	38	67
1200	2.897	116.4	214.6	2.62	67	138	2.7	66.9	222.8	2.4	50	138
1300	2.944	96.4	219.0	2.72	60	145	2.83	78.8	360	2.59	69	189

4. Conclusions

The following conclusions can be drawn from the present study:

(1) This study show that hydroxyapatite powders can be obtained from meleagris gallopova.
(2) In the present study, the results show that the sintering temperature is a critical factor for microstural and mechanical properties of MGHA.
(3) The optimum sintering temperature for MGHA was found to be 1200°C. The measured properties at this temperature were as follows: relative density of >91% dense and has an average grain size of about 8.8 μm, hardness value of 2.12 ± 0.023 GPa, compression value of 116.4 ± 4.46 MPa and fracture toughness value of 0.93 ± 0.10 MPa $\cdot$ m$^{1/2}$, respectively.
(4) Decomposition of MGHA occurred at 1300°C in two ways, one of which is the formation of TCP and the other is CaO.
(5) Due to the decomposition of MGHA at 1300°C, formation of microcracks were observed which may related to much larger difference in coefficient of thermal expansion (CTE) between second (TCP) or calcium oxide (CaO) phases and HA.

Acknowledgements

The authors would like to thank Banvit Company (Izmir, Turkey), Ozlem Cetin, Yakup Karahanli and Abdullah Ozdemir for their support during experimental studies. This work was supported by the Scientific Research Project Program of Marmara University (Project No. FEN-D-040712-0288).

References

[1] F.N. Oktar, Microstructure and mechanical properties of sintered enamel hydroxyapatite, *Ceramics International* **33** (2007), 1309–1314.
[2] C.Y. Ooi, M. Hamdi and S. Ramesh, Properties of hydroxyapatite produced by annealing of bovine bone, *Ceramics International* **33** (2007), 1171–1177.
[3] N. Demirkol, O. Meydanoglu, H. Gokce, F.N. Oktar and E.S. Kayali, Comparison of mechanical properties of sheep hydroxyapatite (SHA) and commercial synthetic hydroxyapatite (CSHA)–MgO composites, *Key Engineering Materials* **493–494** (2012), 588–593.
[4] W. Suchanek, M. Yashima, M. Kakihana and M. Yoshimura, Hydroxyapatite ceramics with selected sintering additives, *Biomaterials* **18** (1997), 923–933.

[5] G.K. Lim, J. Wang, S.C. Ng, C.H. Chew and L.M. Ganl, Processing of hydroxyapatite via microemulsion and emulsion routes, *Biomaterials* **18** (1997), 1433–1439.
[6] M.R. Saeri, A. Afshar, M. Ghorbani, N. Ehsani and C.C. Sorrell, The wet precipitation process of hydroxyapatite, *Materials Letters* **57** (2003), 4064–4069.
[7] A. Afshar, M. Ghorbani, N. Ehsani, M.R. Saeri and C.C. Sorrell, Some important factors in the wet precipitation process of hydroxyapatite, *Materials and Design* **24** (2003), 197–202.
[8] M.-F. Hsieh, L.-H. Perng, T.-S. Chin and H.-G. Perng, Phase purity of sol–gel-derived hydroxyapatite ceramic, *Biomaterials* **22** (2001), 2601–2607.
[9] D.-M. Liu, Q. Yang, T. Troczynski and W.J. Tseng, Structural evolution of sol–gel-derived hydroxyapatite, *Biomaterials* **23** (2002), 1679–1687.
[10] H. Eshtiagh-Hosseini, M.R. Housaindokht and M. Chahkandi, Effects of parameters of sol–gel process on the phase evolution of sol–gel-derived hydroxyapatite, *Materials Chemistry and Physics* **106** (2007), 310–316.
[11] R. Ramachandra Rao, H.N. Roopa and T.S. Kannan, Solid state synthesis and thermal stability of HAP and HAP-β-TCP composite ceramic powders, *Journal of Materials Science: Materials in Medicine* **8**(8) (1997), 511–518.
[12] S. Jinawath, D. Pongkao, W. Suchanek and M. Yoshimura, Hydrothermal synthesis of monetite and hydroxyapatite from monocalcium phosphate monohydrate, *International Journal of Inorganic Materials* **3** (2001), 997–1001.
[13] X. Zhang and K.S. Vecchio, Hydrothermal synthesis of hydroxyapatite rods, *Journal of Crystal Growth* **308** (2007), 133–140.
[14] M. Sivakumar, T.S. Sampath Kumar, K.L. Shantha and K. Panduranga Rao, Development of hydroxyapatite derived from Indian coral, *Biomaterials* **17**(17) (1996), 1709–1714.
[15] E.M. Rivera, M. Araiza, W. Brostow, V.M. Castaño, J.R. Dĩaz-Estrada, R. Hernandez and J. Rogelio Rodrĩguez, Synthesis of hydroxyapatite from eggshells, *Materials Letters* **41** (1999), 128–134.
[16] S.-C. Wu, H.-C. Hsu, Y.-N. Wu and W.-F. Ho, Hydroxyapatite synthesized from oyster shell powders by ball milling and heat treatment, *Materials Characterization* **62** (2011), 1180–1187.
[17] N. Demirkol, Ü. Karaçaylı, L.S. Özyeğin, E.S. Kayalı, F.N. Oktar, O. Gündüz and S. Agathopoulos, A novel hydroxyapatite: Sheep bone derived hydroxyapatite (SHA), in: *4th National Conference of the Hellenic Society of Biomechanics Abstract Book*, 2010, p. 126 (No. 324).
[18] A.M. Janus, M. Faryna, K. Haberko, A. Rakowska and T. Panz, Chemical and microstructural characterization of natural hydroxyapatite derived from pig bones, *Microchim. Acta* **161** (2008), 349–353.
[19] M. Boutinguiza, J. Pou, R. Comesaña, F. Lusquiños, A. de Carlos and B. León, Biological hydroxyapatite obtained from fish bones, *Materials Science and Engineering C* **32** (2012), 478–486.
[20] N.A.M. Barakat, M.S. Khil, A.M. Omran, F.A. Sheikhd and H.Y. Kim, Extraction of pure natural hydroxyapatite from the bovine bones bio waste by three different methods, *Journal of Materials Processing Technology* **209** (2009), 3408–3415.
[21] E. Kusrini and M. Sontang, Characterization of X-ray diffraction and electron spin resonance: Effects of sintering time and temperature on bovine hydroxyapatite, *Radiation Physics and Chemistry* **81** (2012), 118–125.
[22] C.Y. Ooi, M. Hamdi and S. Ramesh, Properties of hydroxyapatite produced by annealing of bovine bone, *Ceramics International* **33** (2007), 1171–1177.
[23] N.A.M. Barakat, K.A. Khalil, F.A. Sheikh, A.M. Omran, B. Gaihre, S.M. Khil and H.Y. Kim, Physiochemical characterizations of hydroxyapatite extracted from bovine bones by three different methods: Extraction of biologically desirable Hap, *Materials Science and Engineering C* **28** (2008), 1381–1387.
[24] D.K. Pattanayak, P. Divya, R.C. Sujal Upadhyay, Parasod, B.T. Rao and T.R. Rama Mohan, Synthesis and evaluation of hydroxyapatite ceramics, *Trends Biomater. Artif. Organs* **18**(2) (2005), 87–92.
[25] J.A. Toque, M.K. Herliansyah, M. Hamdi, A. Ide-Ektessabi and M.W. Wildan, The effect of sample preparation and calcination temperature on the production of hydroxyapatite from bovine bone powders, *IFMBE Proceedings* **15** (2007), 152–155.
[26] F.N. Oktar, Hydroxyapatite–TiO_2 composites, *Materials Letters* **60** (2006), 2207–2210.
[27] G. Muralithran and S. Ramesh, The effects of sintering temperature on the properties of Hydroxyapatite, *Ceramics International* **26** (2000), 221–230.
[28] N. Ozgür Engin and A. Cüneyt Tas, Manufacture of macroporous calcium hydroxyapatite bioceramics, *Journal of the European Ceramic Society* **19** (1999), 2569–2572.
[29] Z. Evis and R.H. Doremus, Effect of YF_3 on hot-pressed hydroxyapatite and monoclinic zirconia composites, *Materials Chemistry and Physics* **105** (2007), 76–79.
[30] R.Z. LeGeros, G. Bonel and R. Legros, Types of "H_2O" in human enamel and in precipitated apatites, *Calcif. Tissue Res.* **26**(2) (1978), 111–118.
[31] M. Nabil Salimi, R.H. Bridson, L.M. Grover and G.A. Leeke, Effect of processing conditions on the formation of hydroxyapatite nanoparticles, *Powder Technology* **218** (2012), 109–118.

[32] A. Krajewski, M. Mazzocchi, P.L. Buldini, A. Ravaglioli, A. Tinti, P. Taddei and C. Fagnano, Synthesis of carbonated hydroxyapatites: efficiency of the substitution and critical evaluation of analytical methods, *Journal of Molecular Structure* **744–747** (2005), 221–228.
[33] S. Mondal, B. Mondal, A. Dey and S.S. Mukhopadhyay, Studies on processing and characterization of hydroxyapatite biomaterials from different bio wastes, *Journal of Minerals & Materials Characterization & Engineering* **11**(1) (2012), 55–67.
[34] L. Berzina-Cimdina and N. Borodajenko, Research of calcium phosphates using Fourier transform infrared spectroscopy, Institute of General Chemical Engineering, Riga Technical University, Latvia.
[35] H.S. Liu, T.S. Chin, L.S. Lai, S.Y. Chiu, K.H. Chung, C.S. Changb and M.T. Luib, Hydroxyapatite synthesized by a simplified hydrothermal method, *Ceramics International* **23** (1997), 19–25.
[36] C.-J. Liao, F.-H. Lin, K.-S. Chen and J.-S. Sun, Thermal decomposition and reconstitution of hydroxyapatite in air atmosphere, *Biomaterials* **20** (1999), 1807–1813.
[37] http://www.bbc.co.uk/weather/745044.
[38] N. Thangamani, K. Chinnakali and F.D. Gnanam, The effect of powder processing on densification, microstructure and mechanical properties of hydroxyapatite, *Ceramics International* **28** (2002), 355–362.
[39] X. Fan, E.D. Case, F. Ren, Y. Shu and M.J. Baumann, Part I: Porosity dependence of the Weibull modulus for hydroxyapatite and other brittle materials, *Journal of the Mechanical behavior of Biomedical Materials* **8** (2012), 21–36.
[40] M. Figueiredo, A. Fernando, G. Martins, J. Freitas, F. Judas and H. Figueiredo, Effect of the calcination temperature on the composition and microstructure of hydroxyapatite derived from human and animal bone, *Ceramics International* **36** (2010), 2383–2393.
[41] Y.W. Gu, N.H. Loh, K.A. Khor, S.B. Tor and P. Cheang, Spark plasma sintering of hydroxyapatite powders, *Biomaterials* **23** (2002), 37–43.
[42] O. Prokopiev and I. Sevostianov, Dependence of the mechanical properties of sintered hydroxyapatite on the sintering temperature, *Materials Science and Engineering A* **431** (2006), 218–227.
[43] F.N. Oktar, S. Agathopoulos, L. Sevgi Ozyegin, O. Gunduz, N. Demirkol, Y. Bozkurt and S. Salman, Mechanical properties of bovine hydroxyapatite (BHA) composites doped with SiO_2, MgO, Al_2O_3, and ZrO_2, *J. Mater. Sci.: Mater. Med.* **18** (2007), 2137–2143.
[44] N. Demirkol, U. Karacayli, O. Gunduz, S. Agathopoulos, S. Salman, E. Sabri Kayali and F. Nuzhet Oktar, A novel biomaterial: Chicken Hydroxyapatite (CHA), European Congress and Exhibition on Advanced Materials and Processes, in: *EUROMAT 2009*, 7–10 September 2009, Glasgow, UK.

Copyright of Bio-Medical Materials & Engineering is the property of IOS Press and its content may not be copied or emailed to multiple sites or posted to a listserv without the copyright holder's express written permission. However, users may print, download, or email articles for individual use.